JOURNAL OF AIRCRAFT
Vol. 46, No. 4, July–August 2009

Numerical Investigation of Circulation Control Airfoils

Byung-Young Min*
Georgia Institute of Technology, Atlanta, Georgia 30332-0150
Warren Lee† and Robert Englar‡
Georgia Tech Research Institute, Atlanta, Georgia 30332-0801
and
Lakshmi N. Sankar§
Georgia Institute of Technology, Atlanta, Georgia 30332-0150

DOI: 10.2514/1.41638

Reynolds-averaged Navier–Stokes simulations are presented for a circulation control airfoil. Comparisons with measured load characteristics are presented. The effects of turbulence models and the spatial accuracy of the simulations on the predictions are examined. It is observed that increasing the spatial accuracy from third-order to seventh-order had only a minor effect on the solution accuracy on the fine grid simulations reported here. Two-equation turbulence models, and particular the κ-ω/κ-ε blended baseline model, tended to perform better than the one-equation model. The predictions were found to be sensitive to the turbulent kinetic energy level of the jet. Inclusion of the plenum chamber and the jet nozzle allowed the physics of the flow to be captured in greater detail than modeling the jet only at the jet slot, but had only a minor influence on the overall loads.

Nomenclature

A_j	=	jet nozzle exit area
C_{DES}	=	constant for detached eddy simulation turbulence model, set to 0.65
C_d	=	drag coefficient
C_l	=	lift coefficient
C_p	=	pressure coefficient
C_μ	=	momentum coefficient
c	=	chord, speed of sound
d	=	distance to the nearest wall
h	=	height
I_{TB}	=	turbulence intensity
M	=	Mach number
$\dot{m}$	=	mass flow rate
P_t	=	total pressure
P_∞	=	freestream static pressure
q_∞	=	freestream dynamic pressure
R	=	gas constant for air
S	=	reference area
T_t	=	total temperature
V_j	=	jet velocity
α	=	angle of attack
γ	=	specific heat ratio

I. Introduction

IN MANY aerospace applications, and in particular for short takeoff and vertical landing (STOVL) applications, there is a need for high-lift systems. This may be achieved using conventional approaches (airfoils augmented with flap and slat devices) or by active flow control (blown flap, circulation control). Among these two approaches (blown flaps and circulation control), circulation control is more effective for a given mass flow rate and energy, because it takes advantage of the Coanda effect to influence the turning of the external potential flow. Circulation control airfoils are mechanically simpler than multi-element airfoils. These active, blown, flow-augmenting devices have far exceeded the high-lift capabilities of mechanical and/or jet flap airfoils. They are also much more effective in high-lift generation than current fluidic devices such as virtual jets, and pulsating fluidic ejection, which are primarily boundary-layer-control devices and are thus limited in their high-lift capability to only that lift which results from reattached flow on the wing with little or no supercirculation. Lifting surfaces on most existing vehicles may be readily retrofitted with circulation control jets, making circulation control an attractive lower weight and mechanically simpler alternative to conventional high-lift systems.

Research personnel at the Georgia Tech Research Institute's (GTRI's) Aerospace Transportation and Advanced Systems Lab, over the past several decades, have been developing and evaluating advanced aerodynamic concepts based on pneumatic circulation control (CC) technology (see [1,2], for example). This experimental research supported by earlier analytical tools led to successful flight demonstrations of these concepts for specific purposes (such as the A-6/CC wing STOL flight demonstrator, documented in [3]). Advanced extreme STOL pneumatic aerodynamic concepts employing circulation control with a desired C_L approaching 10 have also been developed and tested by Eppel et al. [4]. However, these specific mission-oriented programs did not provide a thorough understanding of the detailed nature, characteristics, governing parameters, and physics of the CC aerodynamic phenomenon, and such is clearly needed.

Basic physical understanding of circulation control has been undertaken by GTRI's Englar [5] and NASA Langley Research Center's Jones et al. [6], where pressure, force, and jet turning measurements on a generic elliptic airfoil, as well as particle image velocimetry investigations of the flowfield around a CC general aviation airfoil were accomplished and shed much light on the aerodynamic phenomena.

Over the past several years, the aforementioned experimental studies at GTRI and NASA have been complimented by coordinated efforts in the first-principles-based modeling of circulation control

Presented as Paper 329 at the 46th AIAA Aerospace Sciences Meeting and Exhibit, Reno, NV, 7–10 January 2008; received 15 October 2008; revision received 14 January 2009; accepted for publication 18 January 2009.

*Graduate Research Assistant, School of Aerospace Engineering. Student Member AIAA.
†Graduate Research Assistant.
‡Principle Research Engineer.
§Regents' Professor, School of Aerospace Engineering. Associate Fellow AIAA.

airfoils and wings (CCW). A variety of structured and unstructured grid analyses have been used in these studies. For a recent compilation of computational and experimental studies in this area, the reviewer is referred to [7]. These analytical methods perform acceptably well for conventional sharp-edged blown airfoils as long as the flow remains well attached, even when relatively low-order turbulence models (Baldwin–Lomax or Spalart–Allmaras) and low-order algorithms (spatially second- or fourth-order algorithms) are used. This is because the jet leaves the airfoil at a clearly defined location (sharp-trailing-edge stagnation point), and the primary effect that must be captured is the Coanda jet effect, which governs the turning of the wall jet. The interplay between the inviscid flow outside the jet and the wall jet effects appear to be adequately captured with existing methods. Figure 1 shows a representative CCW section that has been tested at GTRI by Englar et al. [8,9], and Fig. 2 shows previously published calculations by the present authors at a fixed angle of attack as the blowing coefficient is progressively increased [10]. It is seen that the calculations accurately reproduce the large increase in the lift coefficient observed in experiments at $\alpha = 0$ deg. However, as the angle of attack increases, the large suction peak at the leading edge associated with the high levels of circulation causes the boundary layer to separate downstream of this suction peak and the airfoil to stall. Current methods do not predict the leading-edge stall well (Fig. 3), but appear to do well up to the onset of separation.

In spite of the progress that has been made in modeling CCW airfoils, more computational and experimental studies are needed to understand this phenomenon and quantify the effects of the flow parameters that influence this phenomenon: jet slot height, pressure, Reynolds number, surface geometry in the vicinity of the wall jet, and the turbulent kinetic energy within the jet. This work was motivated by this need. A companion experimental database that includes field data is also needed to further calibrate analytical prediction tools. This database is under development under a cooperative experimental program involving GTRI and NASA researchers.

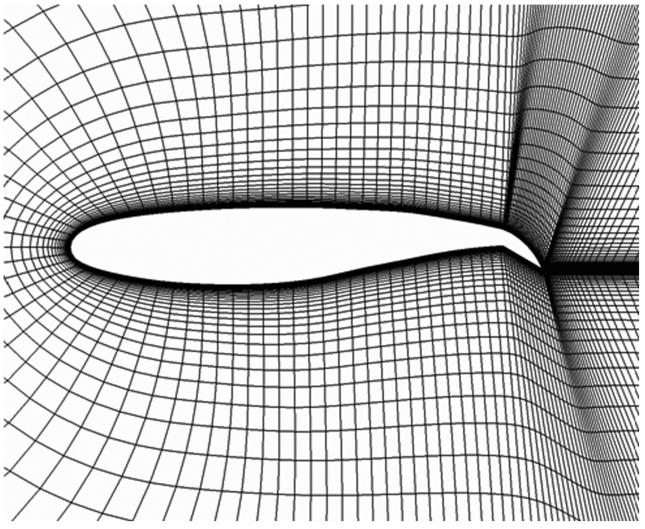

Fig. 1 CCW airfoil with a 30 deg flap.

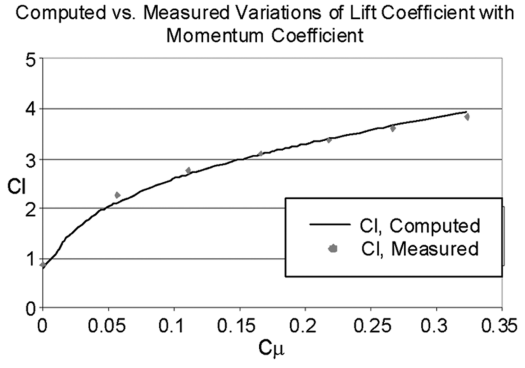

Fig. 2 Comparison of computed and measured results for the CCW airfoil shown in Fig. 1 [10].

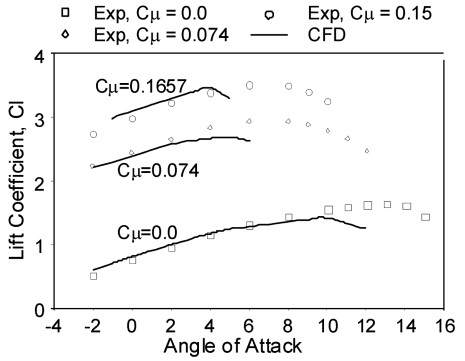

Fig. 3 Variation of the lift coefficient with angle of attack for the CCW configuration, comparisons of predictions (Liu et al. [10]) and measurements (Englar et al. [8]).

First-principles-based numerical studies have been performed for aerodynamic analyses of a pneumatic airfoil NCCR 1510-7067N circulation control (CC) airfoil documented in [11] and shown in Fig. 4. An accurate estimate of the eddy viscosity properties of the Coanda jet requires an accurate estimate of the vorticity in the wall shear layer. High-order accuracy schemes may be needed to reduce the inherent numerical viscosity in low-order spatial accuracy schemes. A comparison of the high-order schemes has been made with the baseline MUSCL scheme to determine what influence, if any, the spatially high-order scheme plays in CCW modeling. A number of turbulence models such as the Spalart–Allmaras (SA) one-equation model, SA-DES (detached eddy simulation), κ-ω/κ-ε blended baseline, and shear stress transport (SST) have been tested. The effects of turbulent kinetic energy level at the jet slot have been assessed. Finally, the effects of modeling the plenum chamber and the jet nozzle have been investigated.

II. Mathematical and Numerical Formulation

All of the results presented here for the NCCR airfoil were generated using the three-dimensional multiblock code Generic Numerical Compressible Airflow Solver (GENCAS). This is a generic Reynolds-averaged Navier–Stokes solver that may be used to model a broad class of internal and external flows. This analysis solves the 3-D compressible Navier–Stokes equations (with 2-D flow as a special case) on a curvilinear body-fitted coordinate system. In this system, the governing equations may be written as follows:

$$\frac{\partial \boldsymbol{Q}}{\partial \tau} + \frac{\partial \boldsymbol{E}}{\partial \xi} + \frac{\partial \boldsymbol{F}}{\partial \eta} + \frac{\partial \boldsymbol{G}}{\partial \zeta} = \frac{\partial \boldsymbol{E}_v}{\partial \xi} + \frac{\partial \boldsymbol{F}_v}{\partial \eta} + \frac{\partial \boldsymbol{G}_v}{\partial \zeta} \tag{1}$$

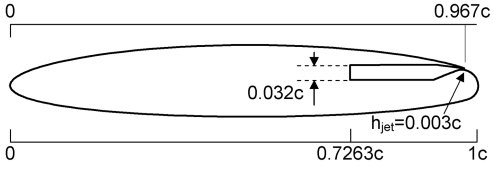

Fig. 4 NCCR 1510-7067N airfoil with plenum.

$$Q=\frac{1}{J}\begin{Bmatrix}\rho\\ \rho u\\ \rho v\\ \rho w\\ e\end{Bmatrix},\qquad E=\frac{1}{J}\begin{Bmatrix}\rho U\\ \rho uU+\xi_x p\\ \rho vU+\xi_y p\\ \rho wU+\xi_z p\\ (e+p)U-\xi_t p\end{Bmatrix}$$

$$F=\frac{1}{J}\begin{Bmatrix}\rho V\\ \rho uV+\eta_x p\\ \rho vV+\eta_y p\\ \rho wV+\eta_z p\\ (e+p)V-\eta_t p\end{Bmatrix}$$

$$G=\frac{1}{J}\begin{Bmatrix}\rho W\\ \rho uW+\zeta_x p\\ \rho vW+\zeta_y p\\ \rho wW+\zeta_z p\\ (e+p)W-\zeta_t p\end{Bmatrix}$$

$$E_v=\frac{1}{JRa}\begin{Bmatrix}0\\ \xi_x\tau_{xx}+\xi_y\tau_{xy}+\xi_z\tau_{xz}\\ \xi_x\tau_{yx}+\xi_y\tau_{yy}+\xi_z\tau_{yz}\\ \xi_x\tau_{zx}+\xi_y\tau_{zy}+\xi_z\tau_{zz}\\ \xi_x\beta_x+\xi_y\beta_y+\xi_z\beta_z\end{Bmatrix}$$

$$F_v=\frac{1}{JRa}\begin{Bmatrix}0\\ \eta_x\tau_{xx}+\eta_y\tau_{xy}+\eta_z\tau_{xz}\\ \eta_x\tau_{yx}+\eta_y\tau_{yy}+\eta_z\tau_{yz}\\ \eta_x\tau_{zx}+\eta_y\tau_{zy}+\eta_z\tau_{zz}\\ \eta_x\beta_x+\eta_y\beta_y+\eta_z\beta_z\end{Bmatrix}$$

$$G_v=\frac{1}{JRa}\begin{Bmatrix}0\\ \zeta_x\tau_{xx}+\zeta_y\tau_{xy}+\zeta_z\tau_{xz}\\ \zeta_x\tau_{yx}+\zeta_y\tau_{yy}+\zeta_z\tau_{yz}\\ \zeta_x\tau_{zx}+\zeta_y\tau_{zy}+\zeta_z\tau_{zz}\\ \zeta_x\beta_x+\zeta_y\beta_y+\zeta_z\beta_z\end{Bmatrix} \tag{2}$$

where

$$\begin{aligned}U&=\xi_t+u\xi_x+v\xi_y+w\xi_z\\ V&=\eta_t+u\eta_x+v\eta_y+w\eta_z\\ W&=\zeta_t+u\zeta_x+v\zeta_y+w\zeta_z\end{aligned} \tag{3}$$

and

$$\begin{aligned}\beta_x&=u\tau_{xx}+v\tau_{xy}+w\tau_{xz}-q_x\\ \beta_y&=u\tau_{yx}+v\tau_{yy}+w\tau_{yz}-q_y\\ \beta_z&=u\tau_{zx}+v\tau_{zy}+w\tau_{zz}-q_z\end{aligned}$$

In these equations, ρ is the density of the air, p is the pressure, u, v, and w are the velocity components, and e is the total energy per unit mass. J is the Jacobian from the coordinate transformation and R_a is the Reynolds number. An upwind scheme was used to approximate the inviscid flux derivatives. This was done using Roe's flux difference splitting. A central difference scheme was used for the calculation of viscous terms. An implicit lower-upper symmetric Gauss–Seidel scheme was employed for time marching.

A. Turbulence Models

The shear stress terms τ_{ij} in Eq. (2) is composed of viscous stress and Reynolds stress components. An eddy viscosity model was used. Thus, the viscosity is the sum of molecular viscosity and eddy viscosity as shown here:

$$\mu=\mu_L+\mu_T$$

In many of the calculations to be presented here, a one-equation transport model for eddy viscosity called the Spalart–Allmaras model [12] was used. Spalart et al. [13] have also proposed a DES model to improve the SA model in separated flows. In the DES model, the turbulence length scale is computed in two different ways. In regions close to the wall, the length scale is related to the closest distance to the wall. In regions away from the wall, this definition is replaced by the maximum cell size as follows:

$$\tilde{d}=\min(d,C_{\mathrm{DES}}\Delta),\qquad \Delta=\max(\Delta x,\Delta y,\Delta z)$$

A second turbulence model used in this study is the κ-ω/κ-ε blended model proposed by Menter [14]. This model combines the best features of the κ-ε and κ-ω models. The κ-ε model tends to overpredict shear stress in the near-wall region because it overestimates the turbulence length scale, thus delaying separation where adverse pressure gradient exists. The κ-ω model, on the other hand, is very sensitive to freestream turbulence levels. In Menter's model, a blending function is used to take advantage of the best features of these two models while minimizing the preceding problems. An eddy viscosity is estimated by the κ-ω model at the near wall, and then the model is gradually switched to κ-ε using a suitable weight function (referred to as κ-ω baseline or BSL). Another improvement of Menter's method over other two-equation models comes from its modified eddy viscosity in the near-wall region where adverse pressure gradient exists (κ-ω SST).

B. High-Order Spatial Accuracy Schemes

For Coanda effects to be modeled, it is critical that the thin wall jet region be accurately captured without excessive numerical dissipation. Conventional third-order upwind schemes and second-order upwind schemes have excessive built-in numerical diffusion which may cause the shear layer to artificially thicken and detach prematurely. To assess the effects of numerical diffusion on the CCW modeling, several high-order upwind schemes [third-order MUSCL, fifth- and seventh-order weighted essentially nonoscillatory (WENO) schemes [15]] have been coded and investigated. In this paper, for brevity, only the conventional approach (third-order upwind scheme) and a high resolution scheme (spatially seventh-order WENO) will be discussed. The fifth-order scheme produced results that lie between the third- and seventh-order schemes discussed here.

III. Circulation Control Airfoil Models and Jet Property Estimation

The circulation control airfoil modeled in this study is the NCCR 1510-7076N airfoil tested at the David W. Taylor Naval Ship Research and Development Center by J. Abramson in 1977 [11]. This is a cambered elliptic airfoil with a thickness-to-chord ratio of 0.15 and a 1% circular arc camber. The airfoil geometry is shown in Fig. 4.

The chord length is 20.34 cm, with the slot position at $0.967c$. A slot height-to-chord ratio (h/c) of 0.003 was selected for current study. The freestream dynamic pressure was 957.6 $\mathrm{N/m^2}$. The freestream static pressure and density were assumed to be 101,325 Pa and 1.216 $\mathrm{kg/m^3}$, respectively. The corresponding freestream Mach number is calculated as 0.116 and the Reynolds number is estimated as 5.45×10^5. The mass flow rate was measured in the experiment but not reported. The jet velocity was estimated as shown in Eq. (4), assuming that the jet velocity increases isentropically as the pressure drops from the total pressure inside the plenum chamber to ambient (freestream) pressure:

Table 1 Estimated mass flow rate

C_μ	0.00	0.025	0.04	0.08	0.12	0.16	0.18	0.209
Mass flow rate, kg/s	0.00	0.0625	0.0794	0.1133	0.1400	0.1630	0.1736	0.1883

$$V_j = \sqrt{2RT_t \frac{\gamma}{\gamma - 1}\left[1 - \left(\frac{p_\infty}{p_t}\right)^{\gamma - 1/\gamma}\right]} \tag{4}$$

The momentum coefficient was then estimated as

$$C_\mu = \frac{\dot{m} V_j}{q_\infty S} \tag{5}$$

Because the momentum coefficient is not a measured value, the actual momentum coefficient at the jet slot differs from the value given in Abramson's report [11]. This discrepancy is possibly due to the use of standard atmospheric conditions in the preceding equations, as opposed to prevailing conditions at the time of the test (not reported).

In view of this discrepancy, it was decided to use mass flow rate as a boundary condition (BC) rather than applying the momentum coefficient directly at the jet slot. The stagnation pressure in the duct is provided by Abramson's report [11], and jet total temperature was assumed the same as the freestream total temperature. Corresponding mass flow rates of several C_μ are given in Table 1. Once the mass flow rate is known, the flow properties at the jet slot can be estimated as follows:

$$\dot{m} = \rho c M A_j, \qquad M = \frac{\dot{m}}{\rho c A_j} \tag{6}$$

Here A_j is the jet exit area. Substituting Mach number into the isentropic relation for total temperature leads to

$$\frac{T_t}{T} = 1 + \frac{\gamma - 1}{2}\left(\frac{\dot{m}}{\rho c A_j}\right)^2 = 1 + \frac{\gamma - 1}{2}\left(\frac{\dot{m}}{A_j}\right)^2 \frac{RT}{\gamma p^2} \tag{7}$$

Rearranging the preceding equation, one gets

$$\frac{\gamma - 1}{2}\left(\frac{\dot{m}}{A_j}\right)^2 \frac{RT^2}{\gamma p^2} + T - T_t = 0 \tag{8}$$

Let

$$\frac{1}{C} = \frac{\gamma - 1}{2}\left(\frac{\dot{m}}{A_j}\right)^2 \frac{R}{\gamma p^2}$$

then the temperature can be obtained as

$$T = \frac{\sqrt{C^2 + 4CT_j} - C}{2} \tag{9}$$

If the jet is subsonic, the static pressure at the jet exit is extrapolated from the interior computational domain. The total temperature of the jet was assumed to be the same as the freestream total temperature, as stated earlier. After the static temperature is obtained, density was calculated from the ideal gas law, and the Mach number from the mass flow rate definition, as follows:

$$\rho = \frac{p}{RT}, \qquad M = \frac{\dot{m}}{\rho c A_j} = \frac{\dot{m}}{\sqrt{\gamma \rho p} A_j} \tag{10}$$

Two different grids with varying resolutions have been tested. Figure 5 shows a relatively low-resolution grid system and Table 2 summarizes the grid dimensions and the associated lift coefficients. Both grid systems use the same two-block topology. The first block wraps around the entire airfoil surface from the jet slot to the upper surface slot lip to make smooth grid at the Coanda surface. A second block (with an O-type grid topology) is then placed outside the surface block. The third block is used only when the plenum chamber is simulated.

The mass flow rate boundary condition described earlier has been applied to the jet slot, and the characteristic-based nonreflecting boundary condition has been applied at the far-field surface. A no-slip condition has been applied at the wall surface with zero gradient of pressure and temperature.

As shown in Table 2, average wall y^+ values of both grids were on the order of 0.1, and computed C_L values were close enough to be

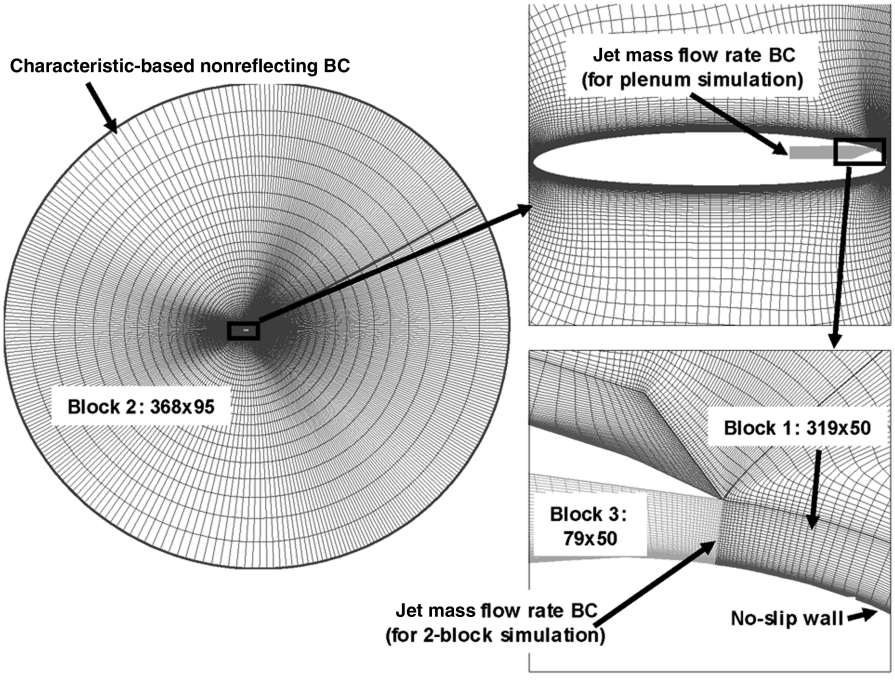

Fig. 5 Details of the body-fitted grid system.

Table 2 Grid test ($C_\mu = 0.209$)

	Grid 1		Grid 2	
	Block 1: 319 × 50	Block 2: 368 × 95	Block 1: 434 × 70	Block 2: 503 × 97
Accuracy	Third-order, k-w SST	Seventh-order, k-w SST	Third-order, k-w SST	Seventh-order, k-w SST
C_l	3.66	3.54	3.63	3.56
Average wall y^+	0.12	0.11	0.10	0.09

considered nearly grid independent. The remainder of the work reported here was done on grid 1.

Some of the calculations reported here were repeated by including the plenum chamber (block 3) and the jet nozzle. Nominal shapes of the plenum chamber and jet nozzle were assumed.

IV. Results and Discussions

Before application of this analysis to CCW sections, the GENCAS solver was extensively validated for conventional airfoil sections (e.g., RAE 2822 airfoil [16]) and for 3-D configurations. These validations are presented in the first author's Ph.D. dissertation [17] and are not included here. Instead, the present study is focused on CCW application.

A systematic study was carried out to assess the effects of the modeling parameters and factors on the predictions. The following issues were examined: 1) formal accuracy of the inviscid flux derivatives, 2) effects of turbulent jet kinetic energy level at the slot exit, 3) inclusion of the plenum and nozzle geometry, and 4) turbulence models. Grid sensitivity studies were also done, as shown in Table 2.

A. Effects of Formal Spatial Accuracy on Computed Loads

As stated earlier, third-order MUSCL schemes, fifth-order weighted essentially nonoscillatory schemes and seventh-order (WENO7) schemes have been implemented in the GENCAS solver. The WENO7 scheme required approximately 20% additional computer time per grid point per time step compared to the standard third-order MUSCL scheme because of the need for determining the weighting coefficients.

Figures 6 and 7 demonstrate the evolution of the lift coefficient with time at two representative values of C_μ. These plots also demonstrate how the three different turbulence models affect the evolution and the nominal steady-state values. Figures 8 and 9 show the representative streamline patterns around the airfoil.

It is observed that increasing the formal accuracy from third-order to seventh-order had only a negligible influence on the global coefficients and flow features, although flow visualizations of the higher-order spatial accuracy solutions (as shown in Fig. 10 for the eddy viscosity levels, directly related to vorticity) appeared to capture the wall jet and the confluent boundary-layer effects more crisply compared to their lower-order counterparts. The computed surface pressure distributions shown in Fig. 11, compared with the experimental data [18], were also relatively insensitive to the formal spatial accuracy of the solution. Field velocity measurements and field turbulence level measurements are needed to determine if the high-order schemes capture these flow features in a quantitatively more accurate manner than lower-order schemes.

B. Effects of Turbulence Level at the Jet Slot on the Solutions

In the experiment, the compressed air from the air supply passes through a supply duct, goes through a plenum chamber (or a setting chamber) before being injected into the external flow at the jet slot. The turbulence level of the jet at the slot exit, and, indirectly, the

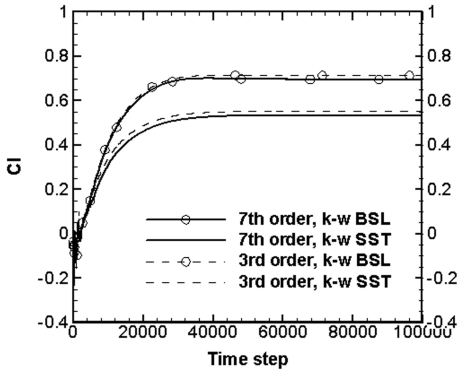

a) C_μ=0.025

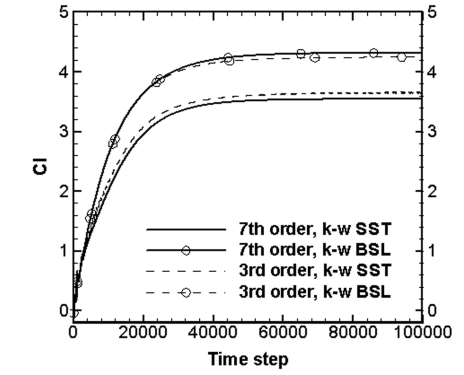

b) C_μ=0.209

Fig. 6 Evolution of lift with time: κ-ω SST and κ-ω BSL.

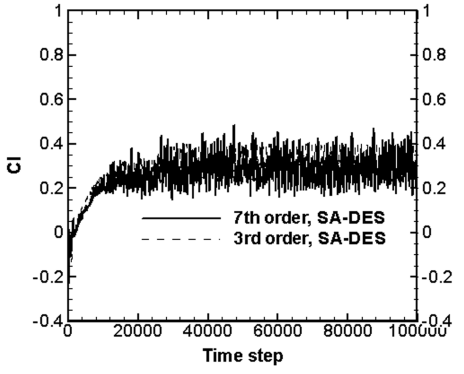

a) C_μ=0.025

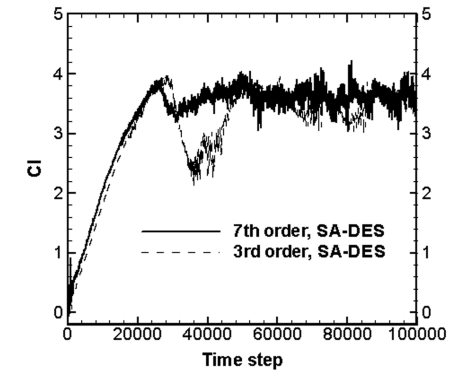

b) C_μ=0.209

Fig. 7 Evolution of lift with time (SA-DES turbulence model).

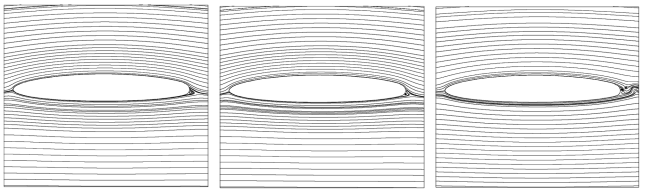

a) κ-ω SST b) κ-ω BSL c) SA-DES

Fig. 8 Instantaneous streamlines at a nominally steady state, $C_\mu = 0.025$.

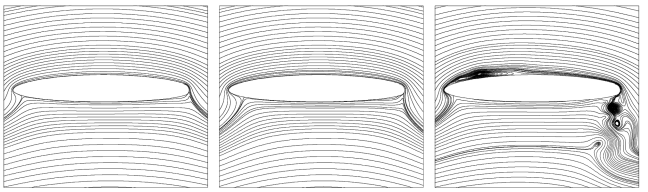

a) κ-ω SST b) κ-ω BSL c) SA-DES

Fig. 9 Instantaneous streamlines at nominal steady state or limit cycle, $C_\mu = 0.209$.

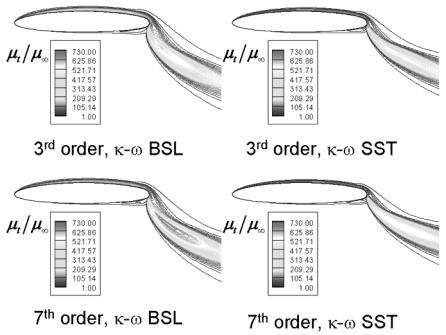

Fig. 10 Eddy viscosity contours, $C_\mu = 0.209$.

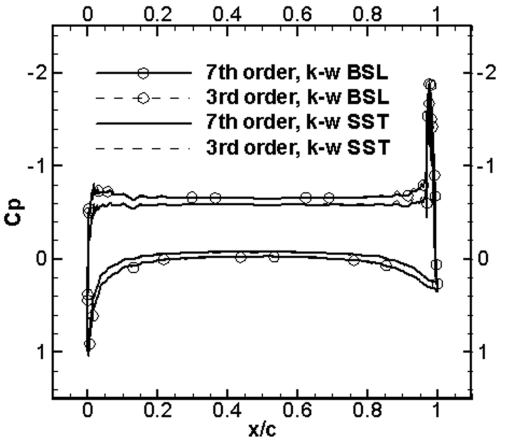

a) C_μ=0.025

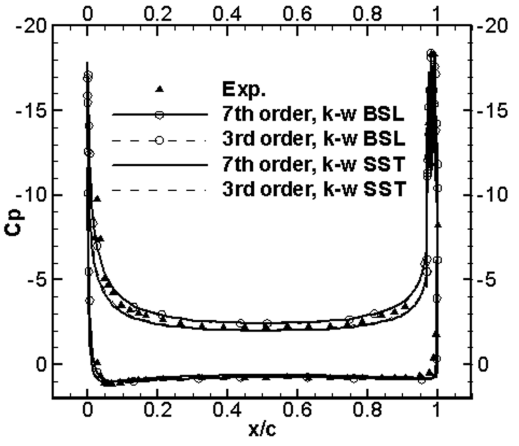

b) C_μ=0.209 (Exp. data from [18])

Fig. 11 Surface pressure distribution.

turbulent kinetic energy of the jet at the slot, may be expected to play a significant role on the subsequent evolution of the jet, the behavior of the confluent boundary layer where the wall jet mixes with the boundary layer over the airfoil upstream of the slot, and eventually the separation of the wall jet off the rounded trailing edge. The separation point may be viewed as a "rear stagnation point" for an equivalent potential flow around the airfoil and determines the circulation around the airfoil and the overall lift.

In the two-equation models and their variant, the κ-ω BSL or κ-ω SST model, the turbulent kinetic energy of the jet may be modeled by setting the "turbulence intensity" to a user-specified value. Because this value was not available from the experimental data, numerical studies were done using two different levels of turbulence intensity (10 and 20% of the mean stream) to assess this effect. As may be expected from the preceding discussions, the jet turbulence level affected the computed loads (shown in Table 3). This study indicates that future CCW experiments should document the turbulent kinetic energy levels of the jet, in addition to the other flow parameters such as C_μ and the flow angle of attack.

C. Effects of Inclusion of Plenum Chamber and Nozzle Geometry on Computed Airloads

Based on the preceding discussions on the turbulent kinetic energy levels of the jet at the slot exit, it may be concluded that the plenum, geometry, and the nozzle geometry may also have an effect on the computed solutions and, in particular, the lift coefficient. Unfortunately, the details of the plenum chamber, the duct supplying air to the plenum, or the nozzle were not available. A notional plenum chamber and nozzle were therefore assumed, and the calculations were done with this configuration at a C_μ of 0.209. The κ-ω SST model was used with the third-order scheme. Figure 12 shows the overall flowfield with and without the inclusion of the plenum chamber. The computed lift coefficients were 3.6242 with plenum and 3.6557 without plenum. Inclusion of the plenum chamber and the jet nozzle produced less than a 1% difference in the computed lift coefficient, and the flow features as shown in Fig. 12 were comparable. It may therefore be concluded that the turbulence levels at the jet slot have more of an effect on the overall solution than the details of the plenum chamber or the nozzle geometry itself.

D. Effects of Turbulence Models on the Computations

A limited number of calculations were done (for several values of C_μ ranging between 0.0 and 0.209) with four turbulence models (SA, SA-DES, κ-ω BSL, and κ-ω SST). Figures 13 and 14 show how the computed lift and drag coefficients were influenced by both the selection of turbulence model and the blowing coefficient. In the experiment, the drag was obtained from wake survey data using a wake deficit method and modified to include additional momentum of the jet, as shown in Eq. (11). The predicted drag was obtained by integrating surface pressure and viscous forces, pressure force at the jet slot, and jet momentum [Eq. (12)]:

Table 3 Effects of jet turbulence levels and plenum chamber on the computed lift coefficient ($C_\mu = 0.209$)

Experiment [11]		Predictions (third-order, κ-ω SST)	
Inlet I_{TB}	——	10%	20%
C_l	4.2	3.5214	3.6557

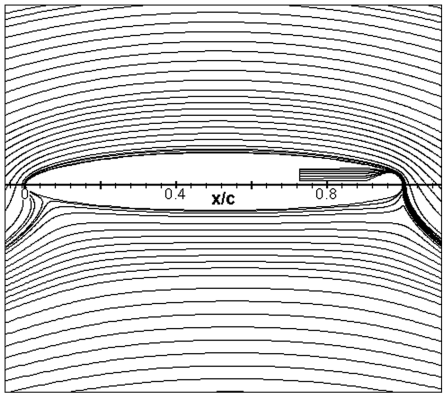

a) With plenum

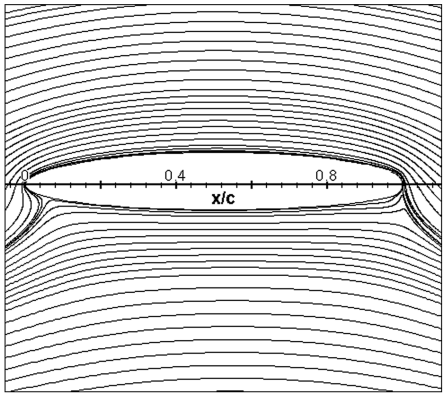

b) Without plenum

Fig. 12 Effects of the inclusion of the plenum chamber on the overall flowfield at $C_\mu = 0.209$.

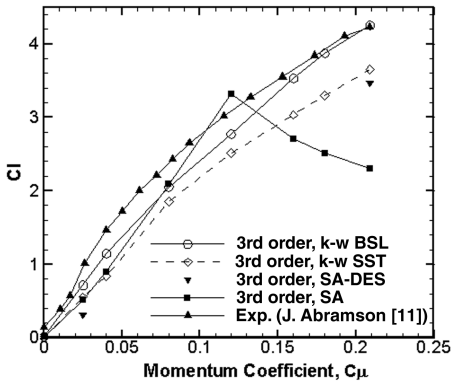

Fig. 13 Effects of turbulence model on the variation of lift coefficient with the momentum coefficient.

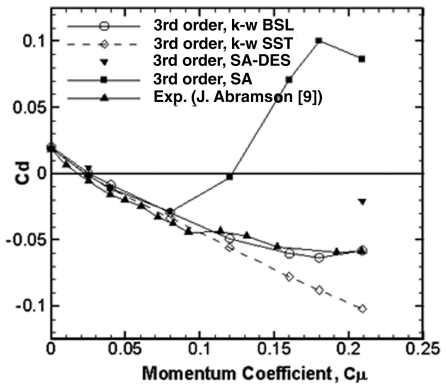

Fig. 14 Effects of turbulence model on the variation of drag coefficient with the momentum coefficient.

$$C_{d_{\text{exp}}} = C_{d_{\text{rake}}} - \frac{\dot{m}V_\infty}{q_\infty S} \tag{11}$$

$$C_{d_{\text{predicted}}} = C_{d_{\text{surface}}} - \frac{\dot{m}V_j + P_j A_j}{q_\infty S} \tag{12}$$

The baseline SA model is the simplest of these models to implement and is quite robust. For the benchmark calculations for the standard AGARD test cases, and for the CCW airfoil with a sharp trailing edge considered in [10], this model proved to be quite effective and adequate. This is partly due to the fact that the sharp trailing edge determines the detachment of the wall jet from the airfoil surface. The SA model, however, relies on a single length scale (namely distance from the nearest wall) for modeling the eddy viscosity. Even the SA-DES model relies on only two characteristic length scales (distance from the wall and computational grid size) for modeling the production and dissipation of turbulent kinetic energy. The CCW problem for blunt airfoils involves at least three length scales: the length scale associated with the wall jet, the length scale associated with the boundary layer upstream of the jet slot, and the length scale associated with the mixing layer where these two shear layers mix and form a thick confluent layer. For this complex problem, the SA model and the SA-DES model predicted a vortex-shedding phenomenon downstream of the trailing edge at low C_μ values (see Figs. 7 and 8), and leading-edge separation followed by leading-edge stall at higher values of C_μ (see Fig. 9). The vortex shedding and leading-edge separation have not been reported in the experiment, however, for this particular incidence angle.

The two-equation models (κ-ω BSL and κ-ω SST) are more costly in terms of implementation and are less robust compared with the SA model. The κ-ω BSL and the κ-ω SST models both use the distance from the wall to switch the models from the near-wall region (where the conventional κ-ω model is used) to a free shear layer region. This switching has proven effective for conventional airfoils where two distinct length scales occur: one near the wall where the length scale is proportional to the distance from the wall, and one away from the wall where the length scale is on the order of boundary-layer thickness. For the CCW cases considered here, the boundary layer downstream of the jet slot is more complex and made of three layers that merge with each other, as stated earlier. Additional work is needed in the area of turbulence modeling for accurate capture of these complex multiscale turbulent flow phenomena. In the present simulations, as seen in Figs. 11b and 13, the κ-ω BSL model did a better job of capturing the overall circulation for the entire range of C_μ considered than the κ-ω SST model. The computed drag values, as shown in Fig. 14, were in good agreement with measurements when the κ-ω BSL model was used. The SA model tended to overestimate drag at higher values of C_μ. No pitching moment measurement was available for the selected case.

V. Conclusions

Reynolds-averaged Navier–Stokes simulations have been done for a circulation control airfoil for a range of momentum coefficients. The effects of grid density, spatial accuracy, upstream turbulence level at the jet slot, and turbulence modeling have been investigated. It was found that turbulence models dramatically affected the wall jet behavior and its detachment point and hence the overall lift and drag value predicted. The turbulence level at the jet slot was also found to have a noticeable influence on the computed solutions. For the grids used in this study, use of high-order spatial accuracy algorithms appeared to achieve an enhanced resolution of the wall jet, boundary layers, and mixing layer, but had a negligible effect on the overall loads. The inclusion of the plenum chamber and the jet nozzle was found to have a negligible effect on the overall loads. Among the turbulence models tested, the κ-ω/κ-ε blended model (referred to as κ-ω BSL) performed the best for the entire range of the momentum coefficient considered.

These conclusions are based on correlations with measured data for the overall lift and drag coefficients for the NCCR airfoil and a sharp trailing-edge airfoil studied previously. For a further assessment of these results, and for improved modeling of the CCW flow phenomena, it is essential that the turbulent flow behavior be characterized through flow visualization and hot-wire measurements of the turbulent flowfield downstream of the jet slot.

Acknowledgments

This work was supported by NASA Langley Research Center under the NASA Grant and Cooperative Research Agreement NNX07AB44A. William E. Milholen is the technical monitor.

References

[1] Englar, R. J., "Overview of Circulation Control Pneumatic Aerodynamics: Blown Force and Moment Augmentation and Modification as Applied Primarily to Fixed-Wing Aircraft," *Proceedings of the 2004 NASA/ONR Circulation Control Workshop*, NASA CP 2005-213509/PT1June 2005, pp. 37–100.

[2] Englar, R. J., and Applegate, C. A., "Circulation Control: A Bibliography of DTNSRDC Research and Selected Outside References (January 1969 through December 1983)," David W. Taylor Naval Ship Research and Development Center DTNSRDC-84/052, Sept. 1984.

[3] Pugliese, A. J., and Englar, R. J., "Flight Testing the Circulation Control Wing," AIAA Paper 79-1791, Aug. 1979.

[4] Eppel, J. G., Shovlin, M. D., Jaynes, D. N., Englar, R. J., and Nichols, J. H., Jr., "Static Investigation of the Circulation-Controlling/Upper-Surface Blowing Concept Applied to the Quiet Short-Haul Research Aircraft," NASA TM-84232, July 1982.

[5] Englar, R. J., "Experimental Investigation of the High Velocity Coanda Wall Jet Applied to Bluff Trailing Edge Circulation Control Airfoils," M.S. Thesis, Dept. of Aerospace Engineering, Univ. of Maryland, College Park, MD, June 1973.

[6] Jones, G. S., Yao, C. S., and Allan, B. G., "Experimental Investigation of a 2D Supercritical Circulation-Control Airfoil Using Particle Image Velocimetry," AIAA Paper 2006-3009, Jan. 2006.

[7] Joslin, R., and Jones, G., *Applications of Circulation Control Technology*, Progress in Astronautics and Aeronautics, Vol. 214, AIAA, Reston, VA, June 2006.

[8] Englar, R. J., Smith, M. J., Kelley, S. M., and Rover, R. C., III, "Application of Circulation Control to Advanced Subsonic Transport Aircraft, Part I: Airfoil Development," *Journal of Aircraft*, Vol. 31, No. 5, Sept. 1994, pp. 1160–1168. doi:10.2514/3.56907

[9] Englar, R. J., Smith, M. J., Kelley, S. M., and Rover, R. C., III, "Application of Circulation Control to Advanced Subsonic Transport Aircraft, Part II: Transport Application," *Journal of Aircraft*, Vol. 31, No. 5, Sept. 1994, pp. 1169–1177. doi:10.2514/3.46627

[10] Liu, Y., Sankar, L. N., Englar, R. J., Ahuja, K., and Gaeta, R., "Computational Evaluation of the Steady and Pulsed Jet Effects on the Performance of a Circulation Control Wing Section," AIAA Paper 2004-0056, Jan. 2004.

[11] Abramson, J., "Two-Dimensional Subsonic Wind Tunnel Evaluation of Two Related Cambered 15-Percent Thick Circulation Control Airfoils," David W. Taylor Naval Ship Research and Development Center ASED-373, Sept. 1977.

[12] Spalart, P. R., and Allmaras, S. R., "A One-Equation Turbulence Model for Aerodynamic Flows," AIAA Paper 92-0439, 1992.

[13] Spalart, P. R., Jou, W.-H., Strelets, M., and Allmaras, S., "Comments on the Feasibility of LES for Wings and on a Hybrid RANS/LES Approach," *Proceedings of the 1st AFOSR International Conference on DNS/LES*, Greyden Press, Columbus, OH, 1997, pp. 137–147.

[14] Menter, F. R., "Two-Equation Eddy-Viscosity Turbulence Models for Engineering Applications," *AIAA Journal*, Vol. 32, No. 8, Aug. 1994, pp. 1598–1605. doi:10.2514/3.12149

[15] Shu, C. W., "Essentially Non-Oscillatory and Weighted Essentially Non-Oscillatory Schemes for Hyperbolic Conservation Laws," *Advanced Numerical Approximation of Nonlinear Hyperbolic Equations*, edited by A. Quarteroni, Vol. 1697, Lecture Notes in Mathematics, Springer, New York, 1998, pp. 325–432.

[16] Cook, P. H., McDonald, M. A., and Firmin, M. C. P., "Aerofoil RAE 2822: Pressure Distributions, and Boundary Layer and Wake Measurements," *Experimental Data Base for Computer Program Assessment*, AGARD, Rept. AR 138, Jan. 1979.

[17] Min, B. Y., "A Physics Based Investigation of Gurney Flaps for Enhancement of Rotorcraft Flight Characteristics," Ph.D. Dissertation (in Preparation), School of Aerospace Engineering, Georgia Inst. of Technology, Atlanta, GA, June 2009

[18] Chang, P. A., Slomski, J., Marino, T., Ebert, M. P., and Abramson, J., "Full-Reynolds Stress Modeling of Circulation Control Airfoils," *Proceedings of the 2004 NASA/ONR Circulation Control Workshop*, NASA CP 2005-213509/PT1June 2005, pp. 141–166.